University of West Bohemia
Faculty of Applied Sciences
Department of Cybernetics

Master's thesis

A tunable pulse generator in eukaryotic gene systems

Pilsen 2019 Anna Sosnová

Prohlášení

Předkládám tímto k posouzení a obhajobě diplomovou práci zpracovanou na závěr studia na Fakultě aplikovaných věd Západočeské univerzity v Plzni.

Prohlašuji, že jsem diplomovou práci vypracovala samostatně a výhradně s použitím odborné literatury a pramenů, jejichž úplný seznam je její součástí.

V Plzni dne 24. května 2019

Anna Sosnová

Declaration

I hereby declare that this master's thesis is completely my own work and that I used only the cited sources.

Acknowledgements

I would like to thank my supervisor and mentor Doc. M.Sc. et M.Sc. Daniel Georgiev, Ph.D., for his guidance and support during my studies and his advice and patience during the work on my theses.
My thanks also go to all my colleagues at Georgiev Lab and employees of XENO Cell Innovations for their support and encouragement.
Finally, I would like to thank my family and my boyfriend for their love, unconditional support and encouragement in all difficult situation.

Abstract

Type 1 incoherent feed-forward loop (I1-FFL), which behaves as a pulse generator, is the most common transcription network motif in both bacteria and yeast. This work proposes a new design of pulse generator in yeast cell induced by pheromone. Pheromone induction is used for activation of the direct path of I1-FFL and also induced dead Cas9 (dCas9) production. dCas9 implemented from the CRISPR-Cas9 system is used for the repression in the indirect path. Mathematical model of the system is introduced and unknown parameters are experimentally identified. 2 mutations of sgRNA are examined and it is shown, that their use changes the dynamic behavior of the system.

Keywords: pulse generator, incoherent feed-forward loop, mathematical model, CRISPR, dCas9, yeast

Abstrakt

Nekoherentní dopředná smyčka typu 1 (I1-FFL), která se chová jako pulzní generátor, je nejběžněji se vyskytujícím typem transkripčních sítí v bakteriích i kvasinkách. Tato práce uvádí nový design pulzního generátoru, který je indukovaný feromonem. Indukce feromonem je použita pro aktivaci přímé dráhy I1-FFL a také pro indukovanou produkci „mrtvé“ Cas9 (dCas9). dCas9, převzaté z CRISPR-Cas9 systému, je použito pro represi v nepřímé dráze. Je představen matematický model navrženého systému a neznámé parametry jsou identifikovány experimentálně. Jsou zkoumány 2 mutace sgRNA a je ukázáno, že jejich použitím dojde ke změně dynamického chování systému.

Klíčová slova: pulzní generátor, nekoherentní dopředná smyčka, matematický model, CRISPR, dCas9, kvasinka

Contents

1 Introduction

This work focuses on design, analysis, and construction of the pulse generator in eukaryotic cells. An incoherent feed-forward loop can serve as a pulse generator. Pulse generator introduced in this theses uses pheromone induction in the direct path and dead Cas9 in the indirect path. Yeast Saccharomyces cerevisiae, one of the most well-known and studied eukaryotic organism, was used in this theses as a model organism.

CRISPR-Cas9 system is highly studied system adapted from naturally occurring immune system in bacteria. It is used for genome editing and thanks to its simple design has high potential in many applications. An adjusted version of the system, which uses dead Cas9 (mutated Cas9 protein), can be used for gene regulation. This work uses dCas9 for repression of pGRR promoter as designed in [1].

The yeast pheromone response pathway is one of the best investigated signaling pathways in yeast. The pathway serves for transduction of extracellular signal in the form of pheromone to the cell nucleus, where a certain set of genes is activated. In the work, it was discovered that pGRR promoter is not only repressed by dCas9 but also activated by pheromone. Another pheromone-induced promoter was also used for regulation of the dCas9 gene. This work uses pheromone induction as the step input of the designed system.

Research of existing studies of CRISPR-Cas9 and single guide RNA structure is described in Chapter 1. Chapter 2 focuses on the characterization of pGRR promoter and design of the actual pulse generator. Possible modification of sgRNA that may influence the dynamic behavior of the pulse are discussed. Next part describes newly introduced mathematical model of the designed system. Previously studied model [2] is used to transform constant pheromone input into new time-dependent input. Chapter 4 focuses on the identification of unknown model parameters using experimentally measured data. 2 modified sgRNA structures were constructed and measured. Parameters related to these changes cannot be directly measured. However, thanks to the pulse generator model, they were indirectly identified using measured data.

2 Biological background

2.1 CRISPR Cas9 system

CRISPR-Cas, short for clustered regularly interspaced short palindromic repeats, was adapted from naturally occurring genome editing system in bacteria, where it serves as an immune system. This defense system provides sequence-specific recognition, targeting, and degradation of exogenous nucleic acid [3]. The core element of CRISPR-Cas is an array of identical DNA repeats separated by spacers. Spacers are derived from foreign genetic elements such as viruses. The repeat-spacer arrays are transcribed and processed into mature RNA, which then forms a complex with Cas protein and guide it toward homologous nucleic acid sequence present in exogenous element (eg. virus), leading to its cleavage [4]. There are six different prokaryotic CRISPR types [5]. This work focused on Type II CRISPR Cas9 system using Streptococcus pyogenes Cas9 protein.

Cas9 is a large 1368-amino-acid long multidomain protein that cuts DNA 3 bp upstream of the PAM sequence. PAM (proto-spacer adjacent motif) is short (2-6bp) sequence that follows the target DNA region and is required for target recognition and cleavage [6]. Cas9 protein consists of two lobes, the alpha-helical recognition lobe (REC) and nuclease lobe (NUC), containing HNH nuclease domain (cleaves the DNA strand complementary to the guide RNA sequence) and RuvC nuclease domain that cleaves DNA strand opposite the complementary strand. Another important part is a C-terminal domain containing PAM-interacting site, which is disordered in Cas9 inactive structure (the apo-Cas9 structure) [7].

Cas9 needs to be assembled with guide RNA in order to recognize and cleave the DNA. Guide RNA can be either native crRNA-tracrRNA or synthetically generated sgRNA (single guide RNA) [8]. Guide RNA contains a 20bp spacer sequence, that is complementary with target DNA. Upon guide RNA binding, Cas9 undergoes a substantial structural rearrangement from an inactive conformation to a DNA recognition-competent conformation [7]. Experiments have shown that Cas9 initiates the target DNA search by probing for proper PAM sequence before searching for potential guide RNA complementarity [9]. Proper target recognition triggers local DNA melting and forming of Watson-Crick base pairing between the guide RNA

and target DNA strand, followed by other structural changes [10]. HNH and RuvC domains than each cleave one strand of the target DNA. The whole process is depicted in Figure 2.1.

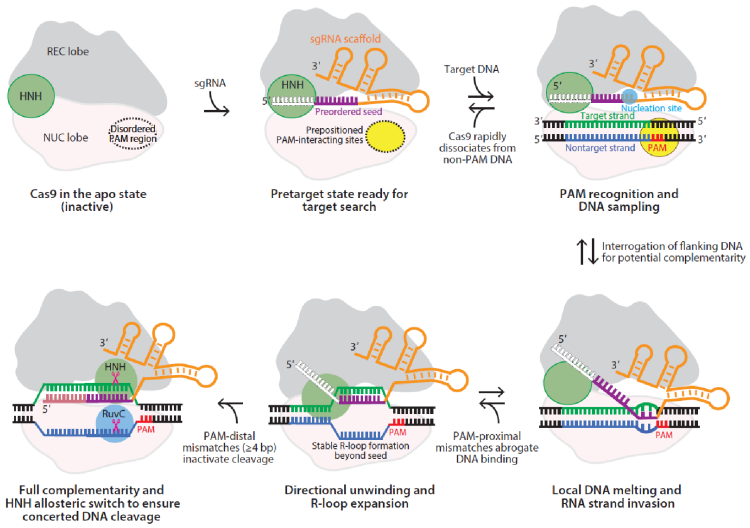

Figure 2.1: Schematic representation of CRISPR-Cas9-mediated target DNA recognition and cleavage [7]

2.2 Single guide RNA (sgRNA)

The guide RNA is an RNA sequence that recognizes the target DNA region and directs there the Cas nuclease for editing. The RNA is made up of two parts, crispr RNA (crRNA), which contain a sequence complementary to the target DNA and tracrRNA, which serves as a binding scaffold for the Cas nuclease [11]. 22 nucleotide sequence of crRNA basepairs with tracrRNA complementary region to form a single structure. Chimeric sgRNA (single guide RNA) is a single transcript, that retains the secondary structure of crRNA:tracrRNA [8].

2.2.1 Structure

sgRNA comprises of 6 different modules: the spacer, the lower stem, the upper stem, the bulge, the nexus, and the harpins [12].

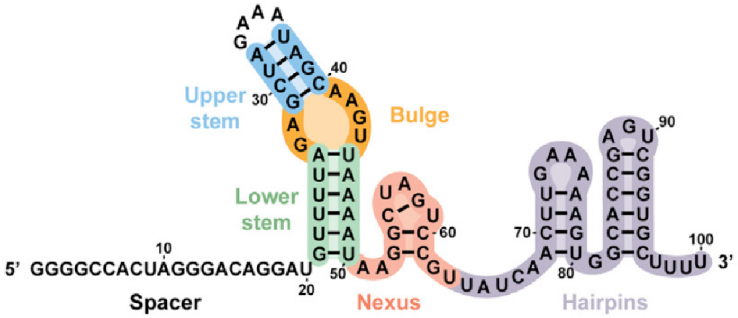

Figure 2.2: sgRNA modules [12]

The 20 nucleotides long spacer sequence determines the location of Cas9 cleavage [8]. 10-12 nt sequence on the 3' end of the spacer is called seed region, which is required for initial DNA interrogation [13]. Cas9 makes interactions with the lower stem, the bulge and upper stem (in some sources also called repeat–antirepeat duplex), and the nexus. It makes much less contact with the harpins and the linker between the nexus and harpins [7] [12].

2.3 Dead Cas9 (dCas9)

Dead Cas9 (dCas9) is a cleavage-inactive form of Cas9, created by mutating both nuclease domains of Cas9 (mutations H840A, D10A). These mutations do not affect the ability to bind DNA but completely abolish endonuclease activity [7]. dCas9 is widely used in CRISPR interference (CRISPRi) and CRISPR activation (CRISPRa) system. These systems serve for gene down-regulation or overexpression respectively [14].

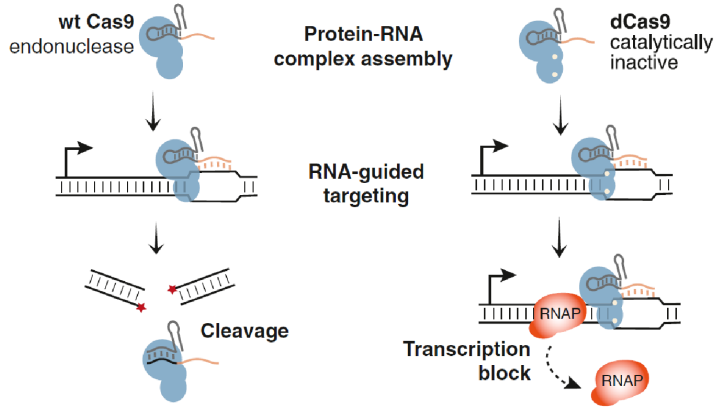

Figure 2.3: Comparison of Cas9 and dCas9 (CRISPRi) activity [14]

In CRISPRi, dCas9 can either repress gene on its own, or it can be fused to other protein repression domains for stronger repression [1]. One of the commonly used domains is KRAB domain (the Krüppel associated box) present in human zinc finger proteins [15]. This work uses dCas9 fused to Mxi1 domain [1], which showed the strongest repression of the pGRR promoter [16].

2.4 Pheromone activated transcription factor Ste12

Yeast Saccharomyces cerevisiae haploid cells use pheromone signaling during their mating process. Following pheromone stimulation, a signal is transmitted through yeast pheromone response pathway from cell membrane to nucleus, resulting in the transcriptional induction of at about 200 genes. Changes in gene expressions are detectable at least 15 minutes after pheromone induction [17]. The Ste12 protein is a transcription factor of these mating genes. In an inactive state, Ste12 is part of Ste12/Dig1/Dig2 complex. Phosphorylated Fus3 and Kss1 proteins phosphorylate Dig1 and Dig2 followed by their unbinding of Ste12 and its activation [18]. There are approximately 1390 molecules of Ste12 in each cell [19] and their number increases after pheromone induction due to positive feedback [20].

Activated Ste12 protein binds as a dimer to PRE element of mating genes promoters [21]. Following table shows some of the PRE sequences reported in the literature. It has been shown that some minor mismatches do not influence Ste12 binding [22].

Table 2.1: Sequences of PRE elements

Sequence	Source
TTGAAACA	[21]
ATGAAAACA	[21]
TGAAACA	[21], [23]
ATGAAC	[24]
ATGAAA	[24]
ATGAAACA	[22]
GGAAACA	[25]

3 Problem definition

3.1 Incoherent feed-forward loop

The incoherent feed-forward loop (IFFL) is a transcription network motif consisting of 2 transcription factors X and Y and one regulated gene Z. When X is active, it binds to a promoter of Z, which initiates the production of protein Z. At the same time, X also activates the production of Y. Y serves as a repressor of promoter Z. When enough molecules of protein Y are produced, the level of protein Z decreases. This type of incoherent feed-forward loop, which has a positive direct path and a negative indirect path, is called the incoherent type 1 feed-forward loop (I1-FFL) [26] [27]. I1-FFL us the most common incoherent configuration in both bacteria and yeast [28].

Transcription occurs when the activator is bound and to a much lesser extent when both the activator and the repressor are present. Therefore, the input function of the promoter is X AND NOT Y [27].

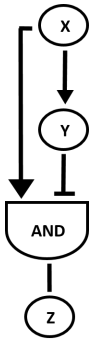

Figure 3.1: Scheme of I1-FFL

Since Z level first increases and then decline to a lower level, the I1-FFL can act as a pulse generator [28].

3.2 Pulse characteristics

Peak

The peak is defined as the maximal value of the pulse.

Peak time

The peak time is the time when the pulse reaches its peak.

Basal level

The basal level is the value of the pulse at time t = 0 min.

Amplitude

This paper defines amplitude as the value of peak minus basal level value.

Final value

The final value is defined as the pulse value at the end of the measurement. It is not necessary the minimal value the pulse can reach.

Rising edge

The rising edge is the pulse transition from low to high.

Falling edge

The falling edge is the pulse transition from high to low.

Rise time

The pulse rise time is the time required for the rising edge of the pulse to go from 10% to 90% of amplitude.

Fall time

The pulse fall time is the time required for the falling edge of the pulse to go from 90% to 10% of amplitude.

Pulse width

The pulse width is the time difference between the 50% amplitudes of the rising and falling edges.

Definitions of the rising edge and the falling edge, the rise time and the fall time and the pulse width are adapted from [29].

3.3 dCas9-Ste12 pulse generator design

The goal is to design a pulse generator in a eukaryotic cell, specifically yeast Saccharomyces cerevisiae. Output of the designed system triggered by a constant input (step input) should have pulse shape. When examining the behaviour of constitutive (constantly active) promoter $pGRR_{5,7}$ (further denoted by pGRR) [16], it was discovered, that its activity is elevated after pheromone induction. This knowledge was not described in the original article.

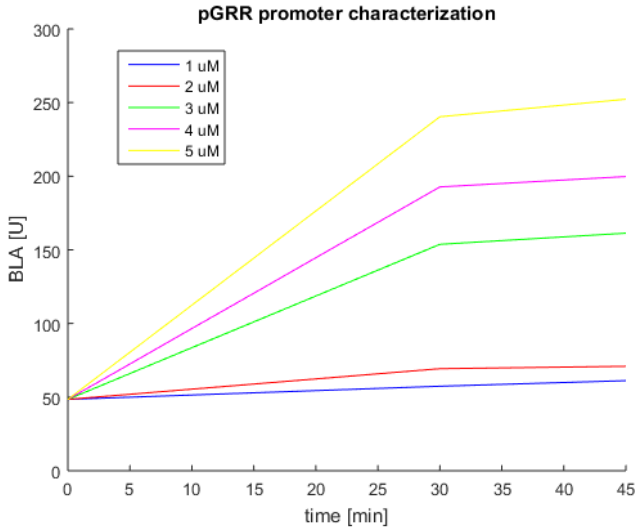

Figure 3.2: pGRR activation after pheromone induction, the value in t = 0 min represents basal promoter activity without pheromone induction

By further examination, there are several potential PRE elements capable of active Ste12 binding. One was directly documented in the literature and two have only minimal mismatch.

Table 3.1: Potential PRE elements of pGRR promoter

pGRR sequence	Location on pGRR	Direction	Reported sequence	Source
ATGAAC	285-290	reverse	ATGAAC	[24]
TGAAAC	367-373	forward	TGAAACA	[21], [23]
ATGCAAC	491-496	forward	ATGAAACA or TGAAACA	[22] [21]

By design, the pGRR promoter can be significantly repressed by dCas9, because it contains two protospacers that can be targeted by sgRNA [16]. Since the promoter can be both activated and repressed, it is suitable for pulse generator design.

The pulse generator is designed as follows

1. Ste12 protein is activated by pheromone
2. pGRR promoter expression is induced by active Ste12

3. dCas9 production is induced by active Ste12 (dCas9 gene is placed downstream of pFIG promoter, that is regulated by Ste12)

4. pGRR promoter is eventually repressed by dCas9

β-lactamase is used as a reporter of pGRR activity.

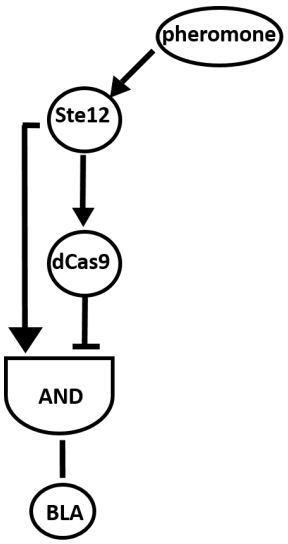

Figure 3.3: Pulse generator scheme

3.4 sgRNA variations

As mentioned before, Cas9 (respectively dCas9) makes contact with some parts of the sgRNA. Therefore, mutations of the sgRNA sequence may influence Cas9 activity. It has been discovered, that alternation of the bulge region abolished Cas9 activity. Complete removal of harpins is required for the same effect, but minor mutations are tolerable [12]. Even though [12] states, that mutations in lower stem and upper stem did not abolish Cas9 activity, a deeper examination of the data shows, that the mutations affect the level of the activity.

This paper examines, how mutations of sgRNA influence dCas9-Mxi1 repression activity. One mutation of the lower stem and one mutation of uppers stem were chosen from article [12]. Lower stem variant introduces double mutation at the base of the lower stem. Upper stem mutant completely removes the upper stem and loop but maintains the bulge structure. Figure 2.7 shows secondary structures of chosen sgRNA mutants. Secondary structures were calculated using mflod tool [30]. Secondary structures were chosen based on their similarity to previously described sgRNA secondary

structure (Figure 2.2). For the control and the lower stem variant, the secondary structures are structures with lowest free energies ($\Delta G = -30.03$ for control and $\Delta G = -27.69$ for lower stem variant), meaning they are considered the most stable ones. Upper stem mutant structure is one with the second lowest free energy $\Delta G = -22.31$ however, this energy is within 5% interval of the lowest energy for this sequence ($\Delta G = -23.43$).

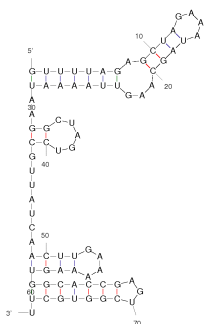

(a) control

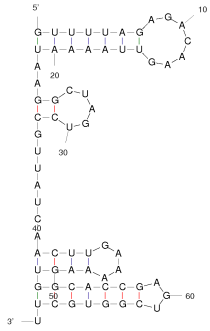

(b) removed upper stem and loop

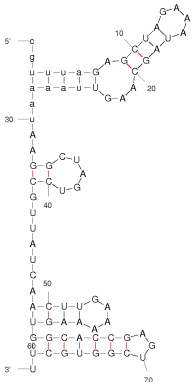

(c) lower stem variant

Figure 3.4: sgRNA secondary structures, calculated using mfold [30]

Table 2.3 summarizes data obtained from the article. Cas9 activity was measured using T7E1 assay in human HEK293 cells. This assay evaluates mutation hit-rate at given locus [31]. Biochemical cleavage was evaluated in vitro using sgRNA, Cas9, and target DNA mixture. AAVS1 and VEGFA are names of used target DNA sequences. The percentage cleavage is defined as a ratio between the sum of area under peaks for cleavage bends, and the sum under both parental and cleavage bends. Meaning, the higher the percentage cleavage, the more effective was the Cas9 targeting.

Table 3.2: Effect sgRNA mutations on Cas9 activity, data from [12]

Type of mutation	Name in article	Cleavage AAVS1	Cleavage VEGFA	Biochemical cleavage
control	control	54	49	92
removed upper stem and loop	GV34	52	35	86
lower stem variant	GV21	19	not reported	92

Data show that in vitro, mutations of sgRNA has minimal effect on Cas9 efficiency. The efficiency of Cas9 seems to be target sequence specific. Upper stem removal decreases Cas9 efficiency by 30% for VEGFA target sequence, however, there is a minimal difference for AAVS1 sequence. Lower stem mutation significantly decreases Cas9 efficiency (to 35%).

Effects of these two mutations on dCas9-Mxi1 activity are further examined in this paper. The hypothesis is, that mutations in sgRNA influence the strength of dCas9 and sgRNA bond, which decreases the repression activity of dCas9. The activity is less influenced by upper stem removal than by lower stem mutation.

4 Modelling

4.1 Yeast pheromone signaling model

Yeast pheromone response pathway has been extensively researched and several models were introduced. Using 35 differential equations, [32] models the whole pathway from Ste2 activation by pheromone to Ste12 targets activation. This model highly simplifies many complex circuits present in the pathway and excludes protein production and degradation. To the contrary, [33] uses more than 70 equations and includes feedback, induced gene expression and translocation of key pathway components.

This work uses a complex yeast pheromone signaling model described in [2] to simulate the behavior of phosphorylated Fus3 (Fus3PP) in response to pheromone induction. This model comprises of approximately 230 rules written in BioNetGen language that include expression, degradation, interactions of proteins, state transformation and several feedback loops. Used rates were obtained from other models or directly observed in yeast. 25% of rates were estimated.

For purposes of this paper, the degradation of pheromone by Bar1 was excluded from the model. 7000s long simulations of the model were performed using alpha factor in a range from 1000 to 10000 molecules (10 nM to 100 nM), concentrations below 1000 molecules showed no response and saturation of the response is reached at approximately 6000 molecules (60nM). Every simulation was performed twice and the mean was calculated since the used NFsim algorithm is stochastic [34].

When compared to measured data, actually used yeast strains are less sensitive to pheromone. At least 1uM of pheromone is required for measurable response and saturation is reached at 5uM of pheromone. Output data of simulations were kept, however, pheromone was rescaled to better corresponded with the measured data.

4.1.1 Fus3PP - transformation of the pheromone input

The aim was to transform input in the form of constant pheromone concentration into new time-dependent Fus3PP input. This simplification of the pathway is acceptable since the main focus of this work is on the pulse generator model which directly follows in Fus3PP. The actual comprehensive

dynamic behavior of all pathway components is therefore insignificant.

Time-dependent changes of Fus3PP were approximated by Gamma distribution probability density function.

$$f(X) = \frac{1}{\Gamma(k)\Theta^k} X^{k-1} e^{-\frac{X}{\Theta}} \tag{4.1}$$

Where random variable X is replaced by time t.

For $k \geq 1$, mode (corresponding to the peak time of Fus3PP) is equal to

$$mode = (k-1)\Theta \tag{4.2}$$

We can obtain normalized function using substitution $X = peakTime$.

$$g(t) = \frac{\frac{1}{\Gamma(k)\Theta^k} \cdot t^{k-1} \cdot e^{-\frac{t}{\Theta}}}{\frac{1}{\Gamma(k)\Theta^k} \cdot peakTime^{k-1} \cdot e^{-\frac{peakTime}{\Theta}}} = \frac{t^{k-1} \cdot e^{-\frac{t(k-1)}{peakTime}}}{peakTime^{k-1} \cdot e^{1-k}} \tag{4.3}$$

Fus3PP(t) function is then multiplication of function g(t) by peak value.

$$Fus3PP(t) = peakValue \cdot \frac{t^{k-1} \cdot e^{-\frac{t(k-1)}{peakTime}}}{peakTime^{k-1} \cdot e^{1-k}} \tag{4.4}$$

Variable parameters $peakValue$ and $peakTime$ are modeled as Hill functions dependent on pheromone concentration. For $peakValue$ the function is increasing with increasing pheromone, for $peakTime$ the function is decreasing.

$$peakTime(pheromone) = a_1 \frac{a_2^{a_3}}{a_2^{a_3} + pheromone^{a_3}} + a_4 \tag{4.5}$$

$$peakValue(pheromone) = b_1 \frac{pheromone^{b_3}}{b_2^{b_3} + pheromone^{b_3}} + b_4 \tag{4.6}$$

Parameters a_1, a_2, a_3, a_4 and b_1, b_2, b_3, b_4 can be easily obtained from yeast pheromone signaling model simulation results using simple fitting algorithm.

Variable shape parameter k is also modeled as Hill function.

$$k(pheromone) = c_1 \frac{pheromone^{c_3}}{c_2^{c_3} + pheromone^{c_3}} + c_4 \tag{4.7}$$

Parameters c_1, c_2, c_3, c_4 were obtained using Matlab fminunc minimization function on Fus3PP simulated data. For more information on used fitting methods see section Fitting methods.

4.1.2 Ste12 activation

In response to pheromone induction, Ste12 negative regulators Dig1 and Dig2 are released from Ste12 protein due to their phosphorylation by Fus3PP, leading to Ste12 activation [35]. Similarly to [33], this complex mechanism was simplified using Hill function, where the rate of Ste12 activation is dependent on Fus3PP concentration. Activated Ste12 is further denoted by Ste12a.

$$v_{18}[t] = \frac{Fus3PP[t]^q \cdot k_1}{k_2^q + Fus3PP[t]^q} \tag{4.8}$$

This approximation does not accurately model the delay in Ste12 activation at higher pheromone concentrations. However, this delay is present in measurement of real yeast cells, where changes in gene expression caused by Ste12a are detectable at least 15 minutes after pheromone induction [17]. It was discovered, that this can be significantly improved by shifting the *peakTime* of Fus3PP in time. This change causes slightly worse approximation of Fus3PP but significantly improves Ste12a approximation. The shift in the peakTime was considered in shape parameter k modeling.

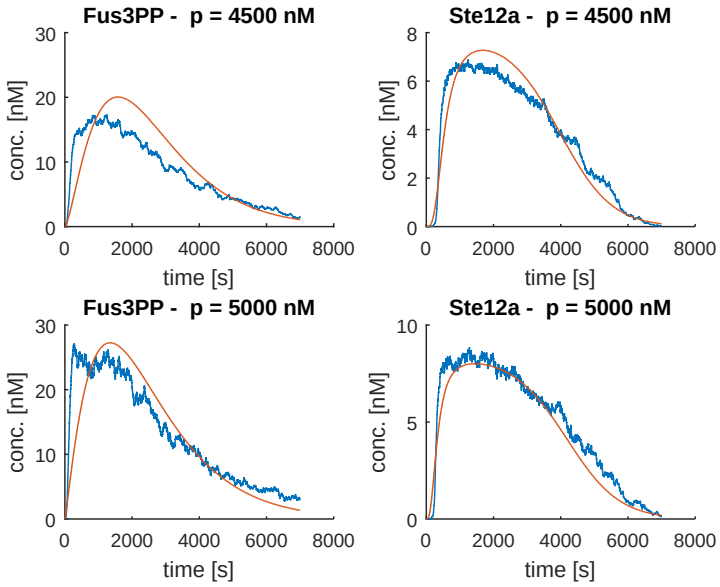

Figure 4.1: Examples of Fus3PP approximation and modeled Ste12 activation, blue lines represent results from Yeast pheromone signaling model, red lines are approximations

4.2 Pulse generator model

In order to model the behavior of design pulse generator and possibly characterize parameters that are not directly measurable, however, have an impact on system behavior, a mathematical model of the pulse generator system was designed.

4.2.1 Model definition

Ste12 activation is dependent on current concentration of Fus3PP.

$$Ste12 \overset{Fus3PP,q,k_1,k_2}{\underset{k_3}{\rightleftharpoons}} Ste12a \tag{4.9}$$

Ste12a binds to PRE region of pFIG1 promoter leading to its activation and expression of dCas9. Cooperativity of Ste12a binding to the promoter is considered. Based on literature search, Ste12a binds to a promoter as a dimer [21], therefore $m = 2$.

$$m \cdot Ste12a + pFIG1 \overset{l_1}{\underset{l_2}{\rightleftharpoons}} Ste12a.pFIG1 \tag{4.10}$$

$$Ste12a.pFIG1 \overset{l_4}{\rightarrow} Ste12a.pFIG1 + dCas9 \tag{4.11}$$

Formation of sgRNA.dCas9 complex is crucial for proper binding to pGRR promoter and its repression.

$$dCas9 + sgRNA \overset{l_{16}}{\underset{l_{17}}{\rightleftharpoons}} sgRNA.dCas9 \tag{4.12}$$

As discovered in this work, Ste12a serves as a transcription factor of pGRR promoter. This promoter also contains spacers allowing sgRNA.dCas9 binding. Cooperativity of Ste12a binding, as well as sgRNA.dCas9 binding to pGRR promoter, was considered. The pulse generator model includes all possible states of pGRR promoter and ways to obtain them.

These are

1. pGRR promoter is not bound by any transcription factor.

2. Ste12a binds to an unoccupied pGRR promoter

$$n \cdot Ste12a + pGRR \overset{l_3}{\underset{l_5}{\rightleftharpoons}} Ste12a.pGRR \tag{4.13}$$

3. sgRNA.dCas9 binds to pGRR promoter, that is already occupied by Ste12a

$$p \cdot sgRNA.dCas9 + Ste12a.pGRR \underset{l_8}{\overset{l_7}{\rightleftharpoons}} sgRNA.dCas9.Ste12a.pGRR \tag{4.14}$$

4. sgRNA.dCas9 binds to unoccupied pGRR promoter

$$p \cdot sgRNA.dCas9 + pGRR \underset{l_{11}}{\overset{l_{10}}{\rightleftharpoons}} sgRNA.dCas9.pGRR \tag{4.15}$$

5. Ste12a binds to pGRR promoter that is already occupied by sgRNA.dCas9

$$n \cdot Ste12a + sgRNA.dCas9.pGRR \underset{l_{15}}{\overset{l_{14}}{\rightleftharpoons}} sgRNA.dCas9.Ste12a.pGRR \tag{4.16}$$

β-lactamase (BLA) is produced on different levels by pGRR promoter in all 4 possible states.

$$Ste12a.pGRR \xrightarrow{l_6} Ste12a.pGRR + BLA \tag{4.17}$$

$$sgRNA.dCas9.Ste12a.pGRR \xrightarrow{l_9} sgRNA.dCas9.Ste12a.pGRR + BLA \tag{4.18}$$

$$sgRNA.dCas9.pGRR \xrightarrow{l_{12}} sgRNA.dCas9.pGRR + BLA \tag{4.19}$$

$$pGRR \xrightarrow{l_{13}} pGRR + BLA \tag{4.20}$$

Degradation of dCas9, sgRNA and β-lactamase is omitted. The total concentration of sgRNA is assumed constant. Initial concentrations of dCas9 and derived complexes are considered zero. The model is described by 11 non-linear ODEs with the same number of state variables. The variables represent the species concentrations in nM per cell.

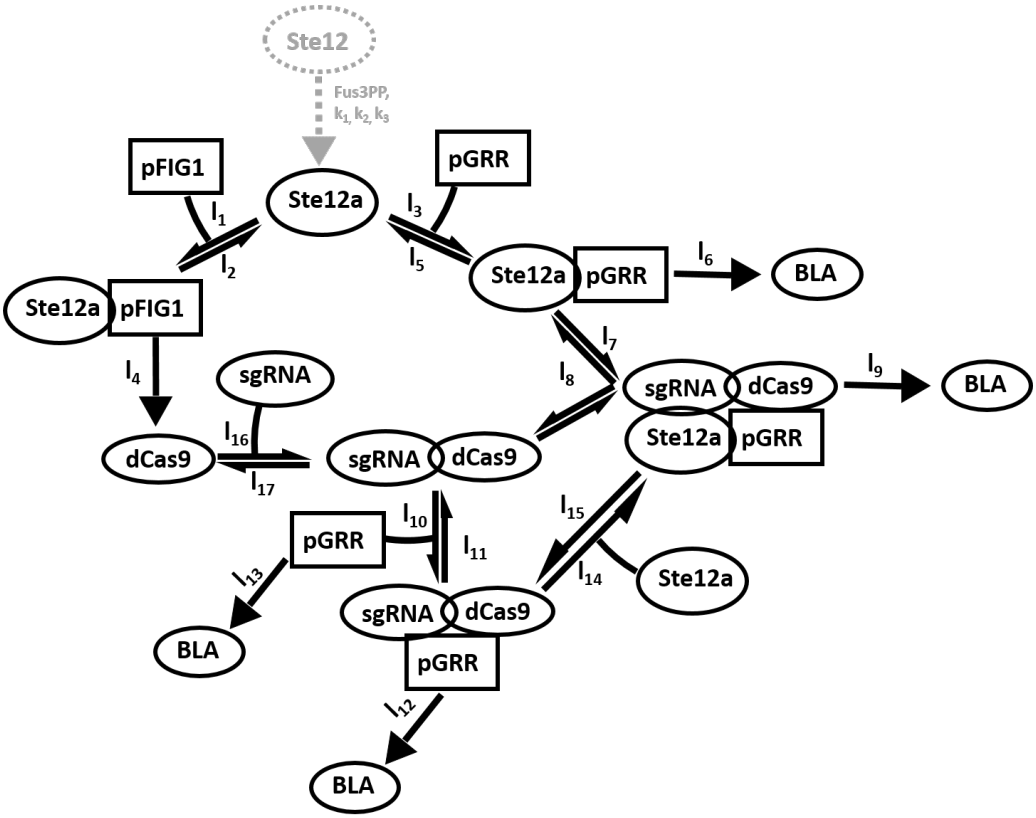

Figure 4.2: Schematic of the system structure. Ste12 activation is indicated, however the non-active Ste12 protein itself is not included in the model.

Table 4.1: Ordinary differential equations

$\frac{dpGRR}{dt} = -v_3 - v_{10} + v_5 + v_{11}$
$\frac{dpFIG1}{dt} = -v_1 + v_2$
$\frac{ddCas9}{dt} = v_4 - v_{16} + v_{17}$
$\frac{dBLA}{dt} = v_6 + v_9 + v_{12} + v_{13}$
$\frac{dsgRNA}{dt} = -v_{16} + v_{17}$
$\frac{dsgRNA.dCas9}{dt} = v_{16} - v_{17} - p \cdot v_7 + p \cdot v_8 - p \cdot v_{10} + p \cdot v_{11}$
$\frac{dSte12a.pGRR}{dt} = v_3 - v_5 - v_7 + v_8$
$\frac{dsgRNA.dCas9.pGRR}{dt} = v_{10} - v_{11} - v_{14} + v_{15}$
$\frac{dsgRNA.dCas9.Ste12a.pGRR}{dt} = v_7 - v_8 + v_{14} - v_{15}$
$\frac{dSte12a}{dt} = v_{18} - v_{19} - m \cdot v_1 + m \cdot v_2 - n \cdot v_3 + n \cdot v_5 - n \cdot v_{14} + n \cdot v_{15}$
$\frac{dSte12a.pFIG1}{d} = v_1 - v_2$

Table 4.2: Rate equations

$v_1 = l_1 \cdot Ste12a[t]^m \cdot pFIG1[t]$
$v_2 = l_2 \cdot Ste12a.pFIG1[t]$
$v_3 = l_3 \cdot Ste12a[t]^n \cdot pGRR[t]$
$v_4 = l_4 \cdot Ste12a.pFIG1[t]$
$v_5 = l_5 \cdot Ste12a.pGRR[t]$
$v_6 = l_6 \cdot Ste12a.pGRR[t]$
$v_7 = l_7 \cdot sgRNA.dCas9[t]^p \cdot Ste12a.pGRR[t]$
$v_8 = l_8 \cdot sgRNA.dCas9.Ste12a.pGRR[t]$
$v_9 = l_9 \cdot sgRNA.dCas9.Ste12a.pGRR[t]$
$v_{10} = l_{10} \cdot sgRNA.dCas9[t]^p \cdot pGRR[t]$
$v_{11} = l_{11} \cdot sgRNA.dCas9.pGRR[t]$
$v_{12} = l_{12} \cdot sgRNA.dCas9.pGRR[t]$
$v_{13} = l_{13} \cdot pGRR[t]$
$v_{14} = l_{14} \cdot Ste12a[t]^n \cdot sgRNA.dCas9.pGRR[t]$
$v_{15} = l_{15} \cdot sgRNA.dCas9.Ste12a.pGRR[t]$
$v_{16} = l_{16} \cdot dCas9[t] \cdot sgRNA[t]$
$v_{17} = l_{17} \cdot sgRNA.dCas9[t]$
$v_{18} = \frac{Fus3PP[t]^q \cdot k_1}{(k_2^q + Fus3PP[t]^q)}$
$v_{19} = k_3 \cdot Ste12a[t]$

In total model has 38 parameters (20 pulse model parameters, 4 Ste12a simulation parameters and 14 parameters approximating Fus3PP). 16 parameters were obtained from literature, 5 parameters were estimated, 12 parameters were calculated and 5 parameters were obtained by fitting to actual data.

See Appendix for parameter values and initial concentrations.

4.2.2 Model in the context of measured data

The output of the model is the expression rate of β-lactamase at each simulation point in one cell. The output of the measurement is the rate of $\Delta_{486-t_0}OD$ change in discrete time points (see Results for more information). In order to fit the model to the measured data, conversion between these two outputs is required.

In the first several minutes, the curve of $\Delta_{486-t_0}OD$ is approximately linear.

$$\Delta_{486-t_0}OD = s \cdot t \tag{4.21}$$

Hydrolysis of nitrocefin by β-lactamase follows Michaelis-Menten kinetics, a model of enzyme kinetics. Under certain assumptions such as that enzyme (β-lactamase) concentration is much lower than substrate (nitrocefin) concentration and the total amount of enzyme is constant, the initial reaction rate is described by Michaelis-Menten equation [36].

$$v_0 = \frac{V_{max}[S]}{k_M + [S]} = \frac{k_{cat}[E_T][S]}{k_M + [S]} \tag{4.22}$$

Where $[S]$ is substrate concentration, $[E_T]$ is total enzyme concentration, k_{cat} constant represents the maximum number of enzymatic reactions catalyzed per second and k_M Michaelis constant. Assuming that concentration of nitrocefin $[N]$ is very high and therefore constant, the initial rate of nitrocefin hydrolysis (production rate of hydrolyzed nitrocefin N^*) is

$$v_{0N^*} = \frac{k_{cat}[N]}{k_M + [N]}[BLA] = M \cdot [BLA] \tag{4.23}$$

Based on previous measurements [37] [38], it is assumed that concentration of hydrolyzed nitrocefin ΔN^* ($\Delta N^* = N^*(t) - N^*(0)$) is linearly dependent on $\Delta_{486-t_0}OD$. Initial concentration of hydrolyzed nitrocefin is close to zero.

$$\Delta N^* = m \cdot \Delta_{486-t_0}OD \tag{4.24}$$

After substitution we get

$$v_{0N^*} \cdot t = m \cdot s \cdot t \tag{4.25}$$

$$[BLA] = \frac{m}{M} \cdot s \tag{4.26}$$

Concentration of β-lactamase in sample is linearly dependent on slope s.

1 unit of β-lactamase (U) can be defined as the amount of enzyme needed to degrade 1nmol of nitrocefin in 1 hour. Absorbance difference 1U resulting

from degradation of 1nmol of nitrocefin was measured to be 0.03. The concentration of β-lactamase in U units can be calculated as

$$[\beta] = \frac{s}{0.03} \tag{4.27}$$

The model simulates the behavior of one cell, however actual measurement reflects a concentration of BLA produced by a sample containing many cells. Using optical density measurement (OD600 = 1), there are approximately $3 \cdot 10^7$ cells in 1 ml [39]. Volume of measured samples V_2 was 100ul, the yeast cell volume V_1 is $29\mu m^{-3}$ [19]. Assuming that [BLA] is a concentration of β-lactamase in the whole sample and [bla] is a concentration of β-lactamase produced by one cell and OD600 is an optical density of the sample, we get

$$[BLA] = OD600 \cdot 3 \cdot 10^7 \cdot \frac{V_1}{V_2} \cdot [bla] \tag{4.28}$$

Presuming that expression rate of β-lactamase P^* is constant in the collection time period Δt, the concentration of produced β-lactamase is equal to

$$[bla] = P^* \cdot \Delta t \tag{4.29}$$

Since OD600 of all samples is normalized to 1, sample volume and used concentration of nitrocefin are kept constant, using several substitutions we get

$$P^* = \frac{[bla]}{\Delta t} = \frac{\frac{[BLA]}{OD600 \cdot 3 \cdot 10^7 \cdot \frac{V_1}{V_2}}}{\Delta t} = \frac{\frac{\frac{m}{M} \cdot \beta \cdot 0.03}{OD600 \cdot 3 \cdot 10^7 \cdot \frac{V_1}{V_2}}}{\Delta t} \tag{4.30}$$

$$\beta = K \cdot P^* \tag{4.31}$$

Amount of β-lactamase β is linearly dependent on expression rate of β-lactamase P^*. Using this equation and only one extra parameter K, the described model can be fitted to data obtained from measurements and therefore developed model corresponds to the actual system.

4.2.3 Approximate production rate

The output of the model is the activation rate P^* of β-lactamase from pGRR promoter at each time point of the solution. Measurements were however obtained only in discrete time point (15 minutes intervals, from 15 minutes after induction to 90 minutes after induction). For simplification, we can assume, that the production rate P^* is constant in the 15 minutes interval. Amount of produced β-lactamase is then

$$[BLA] = \bar{P^*} \cdot t \tag{4.32}$$

We can calculate this approximate rate $\bar{P^*}$ using linear regression on β-lactamase curve of the model, assuming that the curve starting point is shifted to zero and collecting time is 15 minutes. The rate is calculated in units nM/h. This rate is then fitted to measured data using the previously derived equation.

$$\beta = K \cdot \bar{P^*} \tag{4.33}$$

Approximate rate $\bar{P^*}$ is our estimate of the rate, that would produce the measured amount of β-lactamase during the collecting time. Actual rate P^* is however not constant in time.

$$\begin{aligned} P^*(t) = l_6 \cdot Ste12a.pGRR(t) + l_9 \cdot sgRNA.dCas9.Ste12a.pGRR(t) \\ + l_{12} \cdot sgRNA.dCas9.pGRR(t) + l_{13} \cdot pGRR(t) \end{aligned} \tag{4.34}$$

Based on the modeling results, it was discovered, that this approximate rate is roughly equal to P^* in the middle of the collection interval (7.5 minutes). The difference is a couple of seconds.
When both measured data and P^* are displayed, the measured data are placed in the middle of the collection interval, because of the proximity of the P^* value equal to $\bar{P^*}$ used for fitting and also because the whole interval was used for $\bar{P^*}$ calculation.

4.3 Fitting methods

For all fitting methods used in this paper, the function for minimization was a function computing mean square error between the estimated values and measured data (or data obtained from previous simulations).

$$f(x) = MSE(Y, \bar{Y}) = \frac{1}{N}\sum_{i=1}^{N}(Y_i - \bar{Y_i})^2 \tag{4.35}$$

Where Y is a vector of estimated values and $\bar{Y}$ is a vector of measured data and N the length of Y (number of intervals).

For example, when fitting the approximate expression rate $\bar{P^*}$ obtained from model to measured amount of β-lactamase β, the function to minimize is

$$f(x) = MSE(K \cdot \bar{P^*}, \beta) \tag{4.36}$$

fminunc

Fminunc is a Matlab function, that finds a minimum of unconstrained multivariable function [40] . It was used in Fus3PP approximation, specifically in k-parameter fitting. Fminunc minimizes function f(x) for given initial conditions x_0 using Quasi-Newton Algorithm.

fmincon

Fmincon is a Matlab function, that finds a minimum of constrained nonlinear multivariable function [41]. This function was used in the pulse generator model fitting to measured data. Fmincon find minimum of function $f(x)$ specified by

- Linear inequality constraint

$$c(x) \leq 0 \tag{4.37}$$

- Linear equality constraint

$$ceq(x) = 0 \tag{4.38}$$

- Nonlinear inequality constraint

$$A \cdot x \leq b \tag{4.39}$$

- Nonlinear equality constraint

$$Aeq \cdot x = beq \tag{4.40}$$

- lower and upper bounds

$$lb \leq x \leq ub \tag{4.41}$$

We can then further specify other options such as stopping criteria, used algorithm and way of displaying results.

One of the stopping criteria is first-order optimality tolerance. First-order optimality is a measure of how close a point it to optimal. The first-order optimality measure must be zero at minimum, but a point with first-order optimality equal to zero is not necessarily a minimum. Which means that first-order optimality is a necessary condition but not a sufficient condition [42].

For an unconstrained problem, the first-order optimality is defined as the infinity norm of gradient $\nabla f(x)$. For a constrained problem, the first-order optimality is more complex. It is based on Karush-Kuhn-Tucker condition, which is analogous to the condition, that gradient must be zero at a minimum, but is modified to take constraints into account [42].

Karush-Kuhn-Tucker condition uses the Lagrangian function

$$L(x, \lambda) = f(x) + \sum \lambda_{g,i} g_i(x) + \sum \lambda_{h,i} h_i(x) \tag{4.42}$$

Vectors λ_g and λ_h are Lagrange multiplier vectors and their length is same as number of constrains.

Karush-Kuhn-Tucker conditions are

$$\nabla L(x, \lambda) = 0 \tag{4.43}$$

$$\lambda_{g,i} g_i(x) = 0, \forall i \tag{4.44}$$

These conditions are then solved by the algorithm.

Minimization algorithm used in this work was **interior-point algorithm**. Following is a summary of [43].

Interior point algorithm uses barrier function (in form of a logarithmic term) to include defined constraints into the minimization problem. Defining the original problem as

$$\min_x f(x), h(x) = 0 \text{ and } g(x) \leq 0 \tag{4.45}$$

Interior point algorithm redefines this problem to

$$\min_{x,s} f_\mu(x,s) = \min_{x,s} f(x) - \mu \sum_i ln(s_i), \text{ subject to } h(x) = 0 \text{ and } g(x) + s = 0, \mu > 0 \tag{4.46}$$

Slack variables s_i correspond to inequality constraints and must be positive. As μ decreases to zero, the minimum of the function f_μ should approach the minimum of f. This redefinition of the problem creates a sequence of equality constrained problems, that are easier to solve than the original inequality-constrained problem.

The solver can now use one of two types of steps at each iteration

- A direct step in (x,s), also called a Newton step
- A conjugate gradient step

At each iteration, the algorithm attempts to decrease a merit function

$$f_\mu(x,s) + \nu \left\| (h(x), g(x) + s) \right\| \tag{4.47}$$

If the attempted step does not decrease the merit function, the step is rejected and the algorithm attempts a new step. The parameter ν can increase with iteration number to force the solution towards feasibility.

In the direct step, a new complex equation derived from Karush-Kuhn-Tucker conditions is defined. This equation uses Hessian H of the Lagrangian of f_μ, Jacobian of the constraint function g, Jacobian of the constraint function h. This equation is then solved and steps Δx and Δs are obtained. If Hessian H is not positive definite, the direct step can not be used and the algorithm attempts the conjugate gradient step.

As the output of minimization, we not only get desired parameters but also the value of function $f(x)$ (mean square error of found solution and actual data), number of iterations, number of performed calculation of function $f(x)$ and the first-order optimality. The output also includes information, whether the optimization process was successful and if not, what was the cause of its termination.

5 Results

5.1 Experimental data measurement

β-lactamase is an enzyme, that can hydrolyze substrates such as nitrocefin. Hydrolyzation of nitrocefin by β-lactamase is accompanied by a color change from yellow to red [44]. This color change can be measured by a spectrophotometric method measuring optical density (OD) of the sample at 486 nm and 700 nm. At 486 nm, hydrolyzed nitrocefin shows the absorbance peak [45]. At 700 nm, the absorbance of the background is measured.

For measurements, yeast strain transformed with pGRR promoter controlling β-lactamase production, corresponding sgRNA and dCas9 on pheromone-inducible promoter pFIG1 were used. See Appendix Materials and methods for detailed plasmid construction. Alpha factor was used as pheromone since used strains were MATa cells.

Yeast samples were grown overnight in YPD medium, diluted into SDC medium in the morning and let grow for another 3 hours. Samples were then normalized to OD600 0.1. Several tubes with $90\,\mu l$ of the normalized sample were prepared. $10\,\mu l$ of alpha factor (Sigma Aldrich) was added into the first tube, to get $4\,\mu M$ (respectively $5\,\mu M$) final concentration of alpha factor in the tube. In 15 minutes the same amount of alpha factor was added to the second tube. In the meantime, all tubes were incubated in $30°C$, slowly rotating. This process of 15 minutes intervals was performed for 75 minutes.

Cells were then spin down at 3000 rpm for 3 minutes and $100\,\mu l$ of new medium containing alpha factor was added. For one of the tubes, this was the first alpha factor induction. Samples were then incubated for 15 more minutes in $30°C$. Tubes were then spin down at 3000 rpm for 4 minutes and $50\,\mu l$ of each supernatant was mixed in with $40\,\mu l$ SDC and $10\,\mu l$ of $1\,mM$ nitrocefin and absorbance at 486 nm (OD486) and 700 nm (OD700) was measured for 45 minutes. These measurements were then multiplied by 2 since the actual β-lactamase in the sample was diluted twice in the measurement.

The remaining sample was vortexed and $20\,\mu l$ of each sample was mixed with $80\,\mu l$ SDC and OD600 was measured. Obtained data were then re-

calculated to correspond to the original sample. Optical density measurement at 600 nm (OD600) was then used for normalization of the nitrocefin hydrolysis data.

For each sample and concentration, this measurement was done in 3 replicates in 3 days.

5.1.1 Data normalization

The optical density of the background OD700 was subtracted from the optical density OD486 corresponding to the hydrolyzed nitrocefin.

$$\Delta_{486}OD = OD486 - OD700 \tag{5.1}$$

Since we are interested in the differences in the change of $\Delta OD486$ among all the samples, we need to shift starting points of these trends to zero. $\Delta_{486}OD$ in time = 0 min of each sample was subtracted from the rest of the $\Delta_{486}OD$ values.

$$\Delta_{486-t_0}OD(t) = \Delta_{486}OD(t) - \Delta_{486}OD(t=0) \tag{5.2}$$

$\Delta_{486-t_0}OD$ data were normalized using OD600 data. Final values therefore correspond to OD600 = 1.

In the first 30 minutes, $\Delta_{486-t_0}OD$ trend is approximately linear. Data were therefore linearly interpolated. Obtained slope s (in units $\Delta_{486}OD/h$) characterize the speed of $\Delta_{486-t_0}OD$ change, which corresponds to the speed of nitrocefin hydrolysis.

As previously described slopes s were transformed to β-lactamase units U.

$$[\beta] = \frac{s}{0.03} \tag{5.3}$$

Mean and standard deviation were calculated from 3 measured replicates.

5.2 Simple β-lactamase production model

The goal is to identify 6 unknown parameters of the pulse generator model:

- l_4 - production rate of dCas9 from Ste12a bound pFIG1 promoter (Ste12a.pFIG1)

- l_6 - production rate of BLA from Ste12a bound pGRR promoter (Ste12a.pGRR)
- l_9 - production rate of BLA from sgRNA.dCas9 and Ste12a bound pGRR promoter (sgRNA.dCas9.Ste12a.pGRR)
- l_{12} - production rate of BLA from sgRNA.dCas9 bound pGRR promoter (sgRNA.dCas9.pGRR)
- l_{13} - production rate of BLA from unbound pGRR promoter
- K - parameter, that scales P^* to β-lactamase concentration β (β-lactamase units)

In order to identify 2 of these 6 parameters (l_{13} and K), a simple model of β-lactamase production from unbound pGRR promoter was developed. This model uses only 1 reaction rule and is described by two ODEs.

$$pGRR \overset{l_{13}}{\rightarrow} pGRR + BLA \tag{5.4}$$

$$\frac{dpGRR}{dt} = 0 \tag{5.5}$$

$$\frac{dBLA}{dt} = l_{13} \cdot pGRR \tag{5.6}$$

Used yeast strain was incubated for 15 minutes in 3 replicates without pheromone and supernatant was used to measure the amount of produced β-lactamase in the same way as described in section Measuring method. The simple model was then fitted to this data. Interior-point algorithm was used, lower bound was set to 0 and upper bound to 1 for parameter l_{13} and infinity for K. First-order optimality tolerance was set to $1 \cdot 10^{-5}$. There were no other constraints. Table 5.1 summarizes obtained results.

Measured β-lactamase concentration was $\beta = 23.55\ U$.

l_{13} $[s^{-1}]$	K	MSE	First-order optimality	$K \cdot \bar{P}^*$	Num. of iterations
0.0234	7.0747	$1.229 \cdot 10^{-11}$	$2 \cdot 10^{-5}$	23.55	6

Table 5.1: Fitting results of parameters l_{13} and K identification

Obtained parameters l_{13} and K are then used is the pulse generator model.

5.3 Pulse generator model identification

Next step was the identification of 4 remaining unknown parameters (l_4, l_6, l_9 and l_{12}).

We assume that:

1. Production of BLA from Ste12a.pGRR is greater than from unbound pGRR promoter

$$l_6 > l_{13} \tag{5.7}$$

2. Production of BLA from Ste12a.pGRR is grater than or equal to the production from sgRNA.dCas9.Ste12a.pGRR

$$l_6 \geq l_9 \tag{5.8}$$

3. Production of BLA from sgRNA.dCas9.pGRR is significantly lower than the production from Ste12a.pGRR

$$l_6 > l_{12} \tag{5.9}$$

These are linear inequality constraints used in minimization. There are no nonlinear constraints or linear equality constraints. We also assume that all parameters are positive, so the lower bound is zero. In order to keep all the parameters in similar scale as the other parameters used in the model and assuming that production rate of protein is within interval $10^{-1} - 10^{1} s^{-1}$ [2], the upper bound was set as 5.

For minimization, the interior-point algorithm was used, setting first-order optimality tolerance to $1 \cdot 10^{-5}$. Two sets of data were used, measured at alpha factor concentrations $4\,\mu M$ and $5\,\mu M$. When using more than $5\,\mu M$ of pheromone, the pulse behavior does not change (saturation was reached). $4\,\mu M$ induction result in peak value, that is approximately 50% of the maximal possible peak. The model was fitted simultaneously to both of these concentrations.

Table 5.2 summarizes obtained results.

l_4 $[s^{-1}]$	l_6 $[s^{-1}]$	l_9 $[s^{-1}]$	l_{12} $[s^{-1}]$	MSE	First-order optimality	Num. of iterations
1.1	1.0433	0.0017	0.9433	121.07	$9.3 \cdot 10^{-7}$	24

Table 5.2: Results of the pulse generator model identification

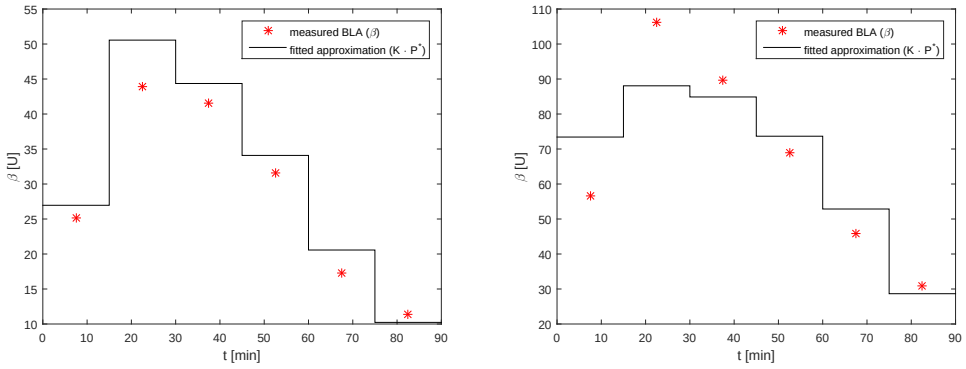

(a) 4000 nM of pheromone (b) 5000 nM of pheromone

Figure 5.1: Approximation of measured data by pulse generator model with identified parameters. Black lines correspond to approximate rate $\bar{P}^*$ multiplied by scaling parameter K. Red stars represent measured data.

Based on obtained parameters, we can conclude that expression of β-lactamase from sgRNA.dCas9 bound pGRR promoter (parameter l_{12}) is significantly lower than the expression from Ste12a bound promoter (parameter l_6). Surprisingly, the results suggest that when both Ste12a and sgRNA.dCas9 are bound to the pGRR promoter, the production of β-lactamase is still quite high (parameter l_9), even though it is lower than production from promoter bound only to Ste12a.
Figure 5.2 shows time development of some state variables. After 4000 nM pheromone induction, we can see, that in the first 25 minutes expression from pGRR is mostly influence by Ste12a, meaning the BLA production is high. sgRNA.dCas9.pGRR reaches 50% of its concentration at around 27 minutes, which is also the time when the pulse (corresponding to 4000nM of pheromone induction) reaches its peak and starts to decrease (Figure 5.3, black curve).
Concentration of sgRNA.dCas9.Ste12a.pGRR is only in 10^{-4} scale, which is 10 times less than Ste12a.pGRR concentration scale and 100 time less than sgRNA.dCas9.pGRR concentration scale. This means that pGRR promoter in state sgRNA.dCas9.Ste12a.pGRR is the least common and production of BLA is less influenced by this state.
5000 nM pheromone induction is followed by a quicker response of the system. More dCas9 is produced. The peak of Ste12a.pGRR is at 9 minutes. sgRNA.dCas9.Ste12a.pGRR influences BLA production more than in case of 4000 nM pheromone induction, however still 10 times less than sgRNA.dCas.pGRR. The pulse shape is also influenced by relatively quick Ste12a deactivation. Such deactivation was predicted by the complex yeast pheromone signaling

model [2], model used for Fus3PP and Ste12a characterization in this work. It is however not clear, whether this deactivation is so quick because this deactivation is slower in other models [32] [33].

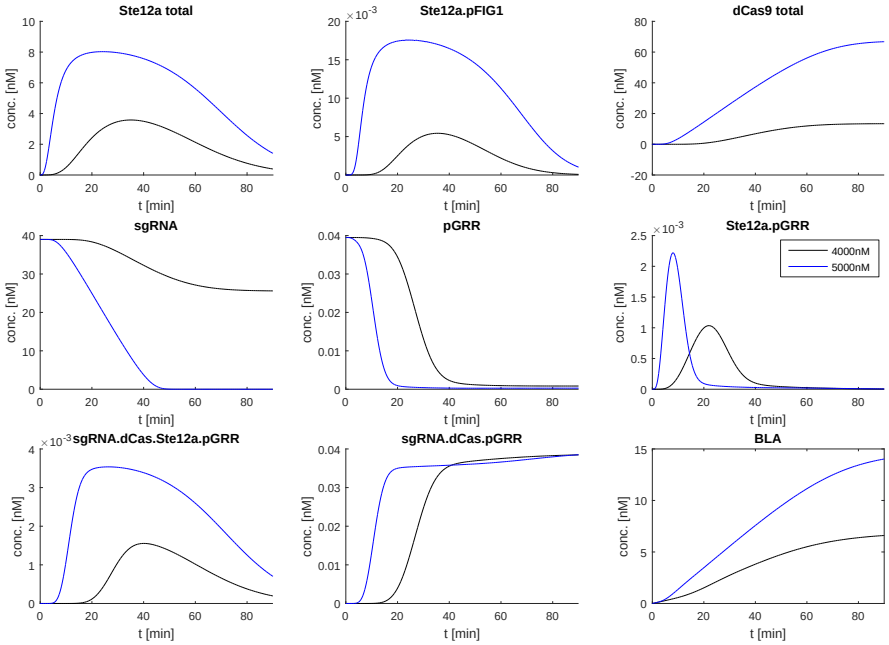

Figure 5.2: Time curves of some state variables of the pulse generator model

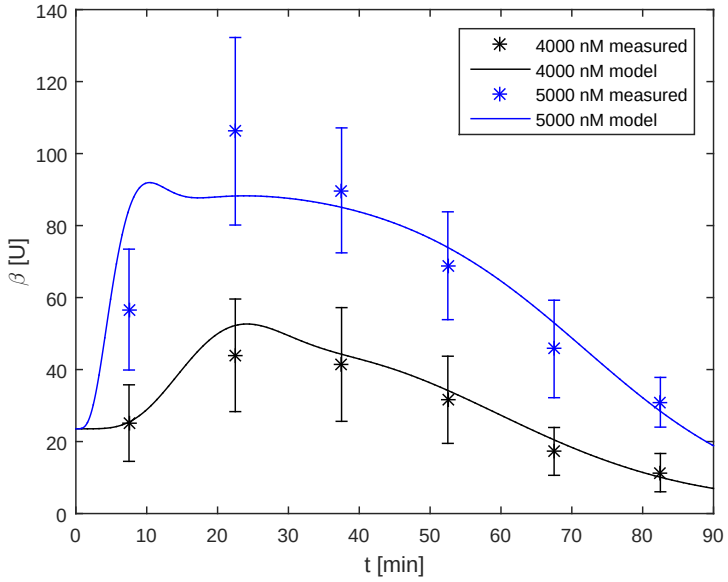

Figure 5.3: Simulation results of BLA production rate P^* (solid lines) multiplied by K, presented together with experimental results (stars).

5.4 Effect of sgRNA variations on pulse dynamics

2 variants of mutated sgRNA were chosen, constructed and transformed into yeast cells. β-lactamase production from these strains after pheromone induction was measured using the same method as in the case of non-mutated sgRNA. Used concentrations of pheromone were $4\,\mu M$ and $5\,\mu M$. 3 replicates were measured and mean and standard deviation were calculated.

In order to identify, how these mutations influence pulse generator response, the pulse generator model was fitted to obtained data. Based on literature research, it was expected, that changes in sgRNA structure influence its binding to dCas9 and possibly also binding of sgRNA.dCas9 to promoter pGRR. Therefore this time, parameters l_4, l_6, l_9, l_{12}, l_{13} and K were kept constant. The fitting process focused on 4 parameters that describe sgRNA, dCas9 a pGRR binding. These are

- l_{16} - association of sgRNA and dCas9 ($1.8 \cdot 10^{-3} nM^{-1} s^{-1}$)
- l_{17} - dissociation of sgRNA.dCas9 ($0\,s^{-1}$)
- l_7 - binding of sgRNA.dCas9 to pGRR promoter ($1 \cdot 10^{-3} nM^{-1} s^{-1}$)
- l_8 - dissociation of sgRNA.dCas9 from pGRR promoter ($2.9 \cdot 10^{-4} s^{-1}$)

Values in parentheses were used in the pulse generator model (using non-mutated sgRNA) and were obtained from the literature (see Appendix for sources). All these parameters cannot be directly measured. However, using the design model, we can identify them indirectly.

When fitting the model to both measured concentration, the MSE was high and the fit was not good for both concentrations. Therefore, fitting was performed only on one concentration of pheromone (4000 nM) and mean square error of simulation results for 5000 nM pheromone was calculated afterward. Based on calculated mean square errors, this leads to good fit for 4000 nM. However, the approximation when using 5000 nM of pheromone is not so good (especially in the case of lower stem mutation).

Interior point algorithm was used, first-order optimality tolerance was set to $1 \cdot 10^{-5}$. Lower bound of all parameters was 0, upper bound was 1. No constraints were used.

5.4.1 Removed upper stem

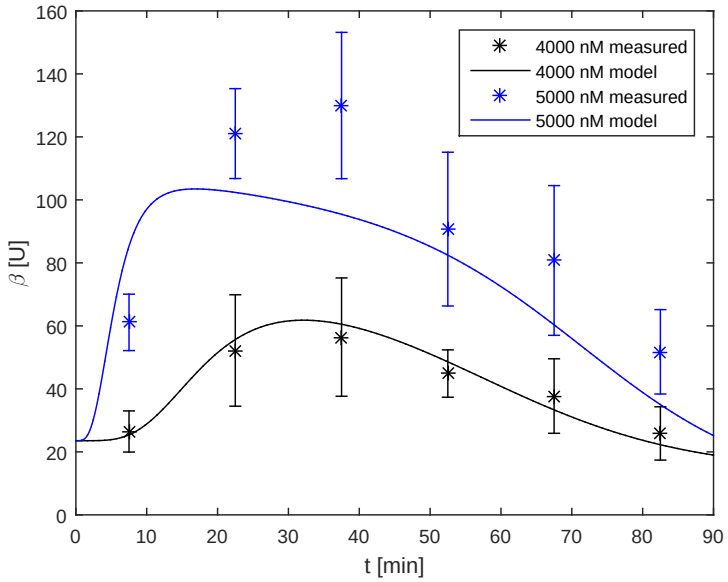

Figure 5.4

Figure 5.4 shows measured β-lactamase produced by strain with sgRNA that has completely removed upper stem. Standard deviation bars are included. Solid lines represent simulated production rate P^* in time multiplied by K. Fitting results are summarized in table 5.3.

l_{16} $[nM^{-1}s^{-1}]$	0.0038	MSE (4000nM)	10.527
l_{17} $[s^{-1}]$	0.0983	MSE (5000nM)	426
l_7 $[nM^{-1}s^{-1}]$	0.0105	First-order optimality	$1 \cdot 10^{-5}$
l_8 $[s^{-1}]$	0.099	Num. of iterations	89

Table 5.3: Fitting results for strain with removed upper stem sgRNA mutation.

Looking at the obtained parameters, we can see that the parameter l_{16}, which corresponds the association of sgRNA and dCas9, remained almost unchanged ($3.8 \cdot 10^{-3}$ vs. original $1.8 \cdot 10^{-3}$). On the other hand, dissociation of sgRNA.dCas9 is present (there was no dissociation in the original model). Both association to and dissociation from the promoter are quicker, particularly the dissociation parameter l_8 is almost 350 times higher, meaning the stability of sgRNA.dCas9.pGRR complex is significantly worse.

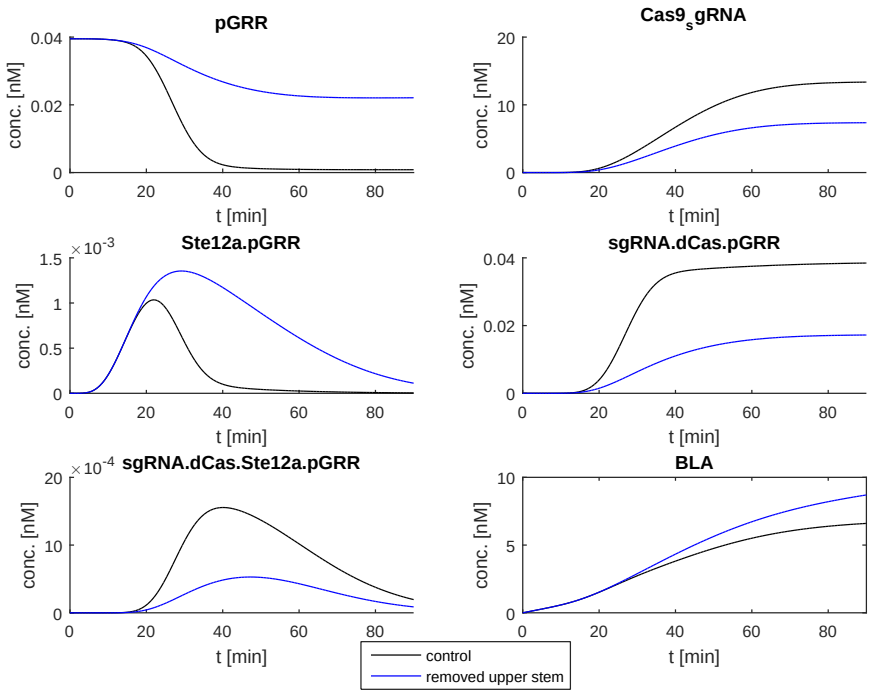

Figure 5.5: Time curves of some state variables of the modified pulse generator model. Result after 4000 nM pheromone induction.

Figure 5.5 shows, that thanks to present dissociation, concentration of sgRNA.dCas9 complex is lower. Ste12a is more often bound to the pGRR promoter on its own, which leads to higher production of β-lactamase. Ste12a.pGRR complex also influences this production later in time, compared to the control (the case when non-mutated sgRNA was used).

5.4.2 Lower stem variant

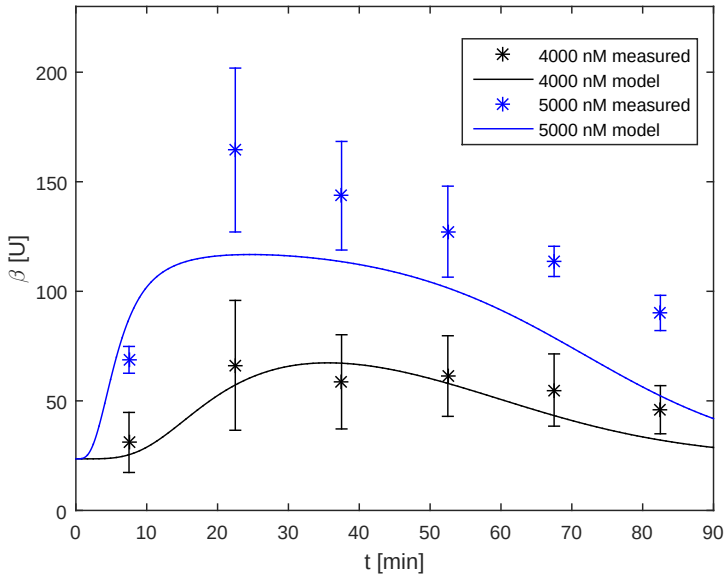

Figure 5.6

Figure 5.6 shows measured β-lactamase produced by strain with sgRNA mutated at the lower stem. Standard deviation bars are included. Solid lines represent simulated production rate P^* in time multiplied by K. Fitting results are summarized in table 5.4.

l_{16} $[nM^{-1}s^{-1}]$	$1.029 \cdot 10^{-5}$	MSE (4000nM)	85.3185
l_{17} $[s^{-1}]$	0.99382	MSE (5000nM)	1110
l_7 $[nM^{-1}s^{-1}]$	0.000317	First-order optimality	$9.8411 \cdot 10^{-6}$
l_8 $[s^{-1}]$	0.99951	Num. of iterations	17

Table 5.4: Fitting results for strain with lower stem variant sgRNA mutation.

Based on the fitting results in Table 5.4, it is obvious that in the case of lower stem mutation, all 4 identified parameters significantly changed. Both the association rate of sgRNA with dCas9 and the association rate of sgRNA.dCas9 to pGRR promoter are lower, which means that both of these processes are slower. In addition to that, both the dissociation of sgRNA.dCas9 from the promoter and the dissociation of the sgRNA.dCas9 complex itself are significantly quicker. All of these changes mean that the sgRNA.dCas9 complex and sgRNA.dCas9.pGRR complex have both very

short duration.
These findings are confirmed in Figure 5.7, where some state variables are shown. The concentration of sgRNA.dCas complex is 10 000 times lower than in case of non-mutated sgRNA (shown in figure 5.5). sgRNA.dCas9 binds pGRR promoter only sporadically, which means that β-lactamase production is almost exclusively influenced by Ste12a.

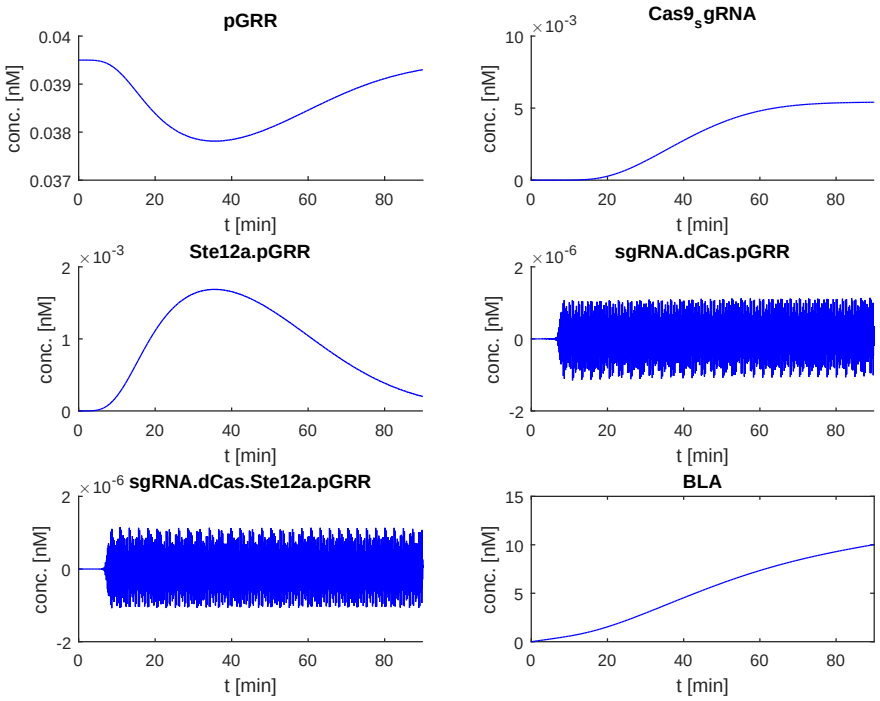

Figure 5.7: Time curves of some state variables of the modified pulse generator model. Result after 4000 nM pheromone induction.

5.4.3 Comparison of pulse characteristics

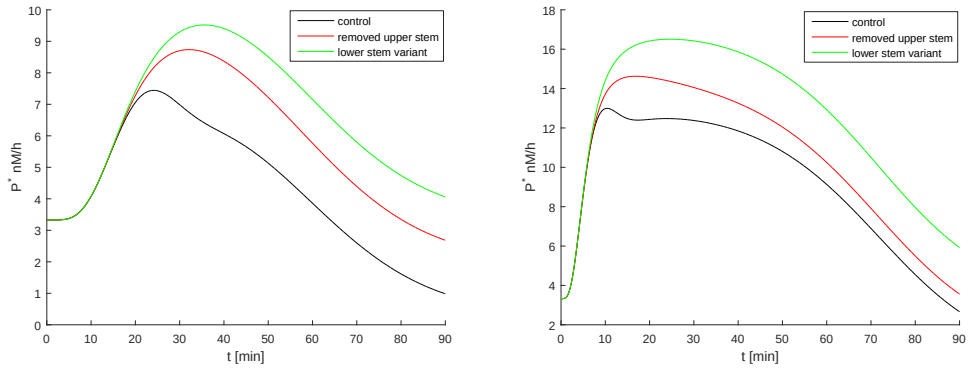

(a) 4000 nM of pheromone (b) 5000 nM of pheromone

Figure 5.8: Comparison of control sgRNA, sgRNA with removed upper stem and sgRNA mutated at lower stem. Lines correspond to BLA production rate P^*.

	control	removed upper stem	lower stem variant
Peak [nM/h]	7.44	8.74	9.52
Peak time	24 min 9 s	32 min	35 min 55 s
Basal level [nM/h]	3.33	3.33	3.33
Amplitude [nM/h]	4.11	5.41	6.19
Final value [nM/h]	0.98	2.68	4.06
Rise time	11 min 32 s	15 min 15 s	16 min 24s
Fall time	31 min 16s	32 min 3 s	$>$ 48 min
Pulse width	33 min 30s	42 min 13 s	48 min 54s

Table 5.5: Pulse characteristics of P^* - 4000 nM of pheromone

Table 5.5 describes pulse characteristics of all 3 examined sgRNA variants after 4000 nM pheromone induction. Model predicts, that the basal level of all 3 variants is the same. This is because the dCas9 initial condition is equal to zero (no leaky production of dCas9 is assumed). Therefore, the change in sgRNA structure does not effect uninduced β-lacatamase production. Actual measurements showed slight vertical shift of the basal level, where the lowest level was obtained for non-mutated sgRNA, the highest for lower stem variant. The differences were however only minor.

Peak time, amplitude and final value are all the lowest when non-mutated sgRNA is used. This confirms, that in this case sgRNA.dCas9 complex is the most stable one and influences β-lactamase production already at peak time. The final value is noticeably lower than in other cases, showing that sgRNA.dCas9 strongly effects β-lactamase later in time.
Maximal peak value, amplitude and the final value were obtained using the lower stem variant of sgRNA. This confirms our hypothesis (based on data from article [12]) that in this case, sgRNA.dCas9 complex is the least stable. This is also supported by the fact, that peak time is not reached until 35 minutes after induction, meaning the sgRNA.dCas9 complex does not affect β-lactamase production earlier in time. During the studied time period, the pulse does not reach back to the basal level, which even further confirms that sgRNA.dCas9 is highly unstable.
sgRNA variant with removed upper stem shows weaker sgRNA.dCas9 activity than non-mutated sgRNA, however still stronger activity than lower stem variant. The final value is lower than the basal level, but the pulse width is almost 10 minutes longer than in case of non-mutated sgRNA, showing that the pulse dynamic is slower.

	control	removed upper stem	lower stem variant
Peak [nM/h]	13	14.63	16.51
Peak time	10 min 20 s	17 min 57 s	24 min 2 s
Basal level [nM/h]	3.33	3.33	3.33
Amplitude [nM/h]	9.67	11.3	13.18
Final value [nM/h]	2.66	3.56	5.92
Rise time	5 min 28 s	6 min 55 s	9 min
Fall time	43 min 49 s	47 min 34 s	$>$ 49 min
Pulse width	59 min 47 s	60 min 20 s	66 min 29s

Table 5.6: Pulse characteristics of P^* - 5000 nM of pheromone

Table 5.6 also shows pulse characteristics, but after 5000 nM of pheromone induction. Since the fitting algorithm was performed using only data after 4000 nM of pheromone induction, results in Table 5.6 are less accurate, especially in the case of lower stem variant, where the MSE of measured data and fitted $\bar{P}^*$ is high. For the control (non-mutated sgRNA) results are more accurate because both pheromone concentrations data sets were used. Nevertheless, data in table 5.6 again confirm, that the lower stem variant

sgRNA forms the weak complex with dCas9. The peak value is the highest, the final value is higher than the basal level, the pulse width is longer than in the other cases. Looking at the actual measured data in Figure 5.6, we can see that the peak is even higher than predicted by the model and also the final value is significantly higher than the basal level.
For all examined variants, the peak is higher, when 5000 nM induction is used. This is in compliance with the fact that more Ste12 is activated and therefore more β-lactamase is produced. The peak is reached quicker than in 4000 nM case. This can be caused either by the higher concentration of Ste12a itself or the fact, that more dCas9 is produced and therefore level of dCas9 required for repression of pGRR is reached quicker.

6 Discussion

This work introduces a new design of the pulse generator in Saccharomyces cerevisiae cells. Pulse generator was designed based on the well-known model of type 1 feed-forward loop. The possibility to activate pGRR promoter (originally designed in [1] as a promoter repressed by dCas9) by pheromone was discovered in this work. This discovery was used in the direct path of the feed-forward loop. Indirect repression path used dCas9 protein fused to Mxi1 repression domain. dCas9 gene was placed downstream of pFIG1 promoter, which is activated after pheromone induction. The whole pulse generator is thus switched on by pheromone addition. The designed generator was constructed and transformed into yeast cells and its output was measured using β-lactamase as a reporter. Output was investigated for 2 concentrations of pheromone used as input.

The behavior of the pulse generator was examined using a newly developed mathematical model. Model input in the form of constant pheromone was transformed into time and pheromone-dependent input in form of phosphorylated Fus3 protein using a previously described model of the yeast pheromone signaling pathway. This transformation is acceptable since our interest lies in the dynamic of the actual pulse generator and not in the complex behavior of the yeast pheromone signaling pathway. Since some of the parameters of the pulse generator model were unknown, experimental data were used for their identification. Expected pulse like behavior was confirmed both experimentally and using the model. It was shown, that the temporal response of the system to a constant step input has pulse like shape.

Furthermore, it was suggested that changes in parameters corresponding to sgRNA binding to dCas9 and their subsequent DNA binding may modify dynamic behavior of the pulse. 2 mutated versions of sgRNA that change its structure were examined. One introduced mutation into the lower stem of sgRNA, the other completely removed upper stem. The negative impact of these mutations on Cas9 activity was previously illustrated [12]. It was expected, that lower stem mutation will have a greater impact on pulse behavior than removal of upper stem. Both structured were incorporated into the pulse generator and output was measured. Using the obtained data, changes in the model parameters were examined. It was shown, that even though these parameters could not be directly measured, the designed model can be used for their identification.

Results showed, that both mutations change the behavior of the pulse generator. Identified model parameters suggest that sgRNA with mutated lower stem forms the least stable complex with dCas9, resulting in weaker repression. Because of it, dCas9 has only a minor impact on β-lactamase production. The peak of the pulse is reached later in time than when non-mutated sgRNA is used and amplitude is greater. Also during the examined period the final value of the pulse does not decrease under the basal level. On the contrary, pulse with non-mutate sgRNA design reached the final value that was lower than the basal level for both used pheromone concentrations.
Removal of the upper stem has also impact on pulse dynamic, however smaller than in the lower stem mutation case. Model parameter corresponding to sgRNA and dCas9 association remains almost unchanged. Other parameters changed, however not so significantly. The final value is lower than the basal level after 4000 nM pheromone induction and equal to the basal level after 5000 nM pheromone induction. Peak time and value are also greater than in the case of non-mutated sgRNA.
In future work, the focus can be on the examination of other possible mutations of sgRNA and their incorporation into the pulse generator. A different model of the complex yeast pheromone signaling pathway can be adapted since the model used in this work shows quicker deactivation of pheromone-induced transcription factor Ste12 than other models. Another improvement of results can be reached by measuring pulse response to more input pheromone concentrations and subsequent model fitting.

Bibliography

[1] Luke A Gilbert, Matthew H Larson, Leonardo Morsut, Zairan Liu, Gloria A Brar, Sandra E Torres, Noam Stern-Ginossar, Onn Brandman, Evan H Whitehead, Jennifer A Doudna, et al. Crispr-mediated modular rna-guided regulation of transcription in eukaryotes. *Cell*, 154(2):442–451, 2013.

[2] Ryan Suderman and Eric J. Deeds. Machines vs. ensembles: Efective mapk signaling through heterogeneous sets of protein complexes. *PLoS Computational Biology*, 9(10), 2013.

[3] Rodolphe Barrangou. The roles of crispr–cas systems in adaptive immunity and beyond. *Current opinion in immunology*, 32:36–41, 2015.

[4] Rodolphe Barrangou. Crispr-cas systems and rna-guided interference. *Wiley Interdisciplinary Reviews: RNA*, 4(3):267–278, 2013.

[5] Kira S Makarova, Yuri I Wolf, Omer S Alkhnbashi, Fabrizio Costa, Shiraz A Shah, Sita J Saunders, Rodolphe Barrangou, Stan JJ Brouns, Emmanuelle Charpentier, Daniel H Haft, et al. An updated evolutionary classification of crispr–cas systems. *Nature Reviews Microbiology*, 13(11):722, 2015.

[6] Francisco JM Mojica, César Díez-Villaseñor, Jesús García-Martínez, and Cristóbal Almendros. Short motif sequences determine the targets of the prokaryotic crispr defence system. *Microbiology*, 155(3):733–740, 2009.

[7] Fuguo Jiang and Jennifer A Doudna. Crispr–cas9 structures and mechanisms. *Annual review of biophysics*, 46:505–529, 2017.

[8] Martin Jinek, Krzysztof Chylinski, Ines Fonfara, Michael Hauer, Jennifer A Doudna, and Emmanuelle Charpentier. A programmable dual-rna–guided dna endonuclease in adaptive bacterial immunity. *Science*, 337(6096):816–821, 2012.

[9] Samuel H Sternberg, Sy Redding, Martin Jinek, Eric C Greene, and Jennifer A Doudna. Dna interrogation by the crispr rna-guided endonuclease cas9. *Nature*, 507(7490):62, 2014.

[10] Fuguo Jiang, David W Taylor, Janice S Chen, Jack E Kornfeld, Kaihong Zhou, Aubri J Thompson, Eva Nogales, and Jennifer A Doudna. Structures of a crispr-cas9 r-loop complex primed for dna cleavage. *Science*, 351(6275):867–871, 2016.

[11] Synthego. *CRISPR101 - Your Guide to Understanding CRISPR.*

[12] Alexandra E Briner, Paul D Donohoue, Ahmed A Gomaa, Kurt Selle, Euan M Slorach, Christopher H Nye, Rachel E Haurwitz, Chase L Beisel, Andrew P May, and Rodolphe Barrangou. Guide rna functional modules direct cas9 activity and orthogonality. *Molecular cell*, 56(2):333–339, 2014.

[13] Fuguo Jiang, Kaihong Zhou, Linlin Ma, Saskia Gressel, and Jennifer A Doudna. A cas9–guide rna complex preorganized for target dna recognition. *Science*, 348(6242):1477–1481, 2015.

[14] Lei S Qi, Matthew H Larson, Luke A Gilbert, Jennifer A Doudna, Jonathan S Weissman, Adam P Arkin, and Wendell A Lim. Repurposing crispr as an rna-guided platform for sequence-specific control of gene expression. *Cell*, 152(5):1173–1183, 2013.

[15] Stuart Huntley, Daniel M Baggott, Aaron T Hamilton, Mary Tran-Gyamfi, Shan Yang, Joomyeong Kim, Laurie Gordon, Elbert Branscomb, and Lisa Stubbs. A comprehensive catalog of human krab-associated zinc finger genes: insights into the evolutionary history of a large family of transcriptional repressors. *Genome research*, 16(5):669–677, 2006.

[16] Miles W Gander, Justin D Vrana, William E Voje, James M Carothers, and Eric Klavins. Digital logic circuits in yeast with crispr-dcas9 nor gates. *Nature communications*, 8:15459, 2017.

[17] Christopher J Roberts, Bryce Nelson, Matthew J Marton, Roland Stoughton, Michael R Meyer, Holly A Bennett, Yudong D He, Hongyue Dai, Wynn L Walker, Timothy R Hughes, et al. Signaling and circuitry of multiple mapk pathways revealed by a matrix of global gene expression profiles. *Science*, 287(5454):873–880, 2000.

[18] Lee Bardwell. A walk-through of the yeast mating pheromone response pathway. *Peptides*, 26(2):339–350, 2005.

[19] Ty M Thomson, Kirsten R Benjamin, Alan Bush, Tonya Love, David Pincus, Orna Resnekov, C Yu Richard, Andrew Gordon, Alejandro

Colman-Lerner, Drew Endy, et al. Scaffold number in yeast signaling system sets tradeoff between system output and dynamic range. *Proceedings of the National Academy of Sciences*, 108(50):20265–20270, 2011.

[20] Joseph W Dolan and Stanley Fields. Overproduction of the yeast ste12 protein leads to constitutive transcriptional induction. *Genes & development*, 4(4):492–502, 1990.

[21] YL Yuan and S Fields. Properties of the dna-binding domain of the saccharomyces cerevisiae ste12 protein. *Molecular and Cellular Biology*, 11(12):5910–5918, 1991.

[22] Gwenael Badis, Esther T Chan, Harm van Bakel, Lourdes Pena-Castillo, Desiree Tillo, Kyle Tsui, Clayton D Carlson, Andrea J Gossett, Michael J Hasinoff, Christopher L Warren, et al. A library of yeast transcription factor motifs reveals a widespread function for rsc3 in targeting nucleosome exclusion at promoters. *Molecular cell*, 32(6):878–887, 2008.

[23] Joseph W Dolan, Celia Kirkman, and Stanley Fields. The yeast ste12 protein binds to the dna sequence mediating pheromone induction. *Proceedings of the National Academy of Sciences*, 86(15):5703–5707, 1989.

[24] Rhonda Harrison and Charles DeLisi. Condition specific transcription factor binding site characterization in saccharomyces cerevisiae. *Bioinformatics*, 18(10):1289–1296, 2002.

[25] Sheetal Raithatha, Ting-Cheng Su, Pedro Lourenco, Susan Goto, and Ivan Sadowski. Cdk8 regulates stability of the transcription factor phd1 to control pseudohyphal differentiation of saccharomyces cerevisiae. *Molecular and cellular biology*, 32(3):664–674, 2012.

[26] Shai Kaplan, Anat Bren, Erez Dekel, and Uri Alon. The incoherent feed-forward loop can generate non-monotonic input functions for genes. *Molecular systems biology*, 4(1):203, 2008.

[27] Uri Alon. *An introduction to systems biology: design principles of biological circuits*. Chapman and Hall/CRC, 2006.

[28] Shmoolik Mangan and Uri Alon. Structure and function of the feed-forward loop network motif. *Proceedings of the National Academy of Sciences*, 100(21):11980–11985, 2003.

[29] Keysight Technologies Inc. *Pulse Parameter Definitions*.

[30] Michael Zuker. Mfold web server for nucleic acid folding and hybridization prediction. *Nucleic acids research*, 31(13):3406–3415, 2003.

[31] Diagenode. *CRISPR/Cas9 editing: mutation detection with mismatch cleavage assay.*

[32] Bente Kofahl and Edda Klipp. Modelling the dynamics of the yeast pheromone pathway. *Yeast*, 21(10):831–850, 2004.

[33] Danying Shao, Wen Zheng, Wenjun Qiu, Qi Ouyang, and Chao Tang. Dynamic studies of scaffold-dependent mating pathway in yeast. *Biophysical journal*, 91(11):3986–4001, 2006.

[34] Michael W Sneddon, James R Faeder, and Thierry Emonet. Efficient modeling, simulation and coarse-graining of biological complexity with nfsim. *Nature methods*, 8(2):177, 2011.

[35] Kerry Tedford, Sammy Kim, Danne Sa, Ken Stevens, and Mike Tyers. Regulation of the mating pheromone and invasive growth responses in yeast by two map kinase substrates. *Current Biology*, 7(4):228–238, 1997.

[36] Michaelis L and Menten M. Kinetik der invertinwirkung biochem. *Biochemische Zeitschrift*, 49:333–369, 1913.

[37] Abcam. *Beta Lactamase Activity Assay Kit*, 3 2015. Version 1.

[38] Guoliang Zhen, Verena Eggli, Janos Vörös, Prisca Zammaretti, Marcus Textor, Rudi Glockshuber, and Eva Kuennemann. Immobilization of the enzyme β-lactamase on biotin-derivatized poly (l-lysine)-g-poly (ethylene glycol)-coated sensor chips: a study on oriented attachment and surface activity by enzyme kinetics and in situ optical sensing. *Langmuir*, 20(24):10464–10473, 2004.

[39] Audra Day, Colette Schneider, and Brandt L Schneider. Yeast cell synchronization. In *Cell Cycle Checkpoint Control Protocols*, pages 55–76. Springer, 2004.

[40] Matlab fminunc. [online]. [cited 2019-05-06] Available at: `https://www.mathworks.com/help/optim/ug/fminunc.html`.

[41] Matlab fmincon. [online]. [cited 2019-05-05] Available at: `https://www.mathworks.com/help/optim/ug/fmincon.html`.

[42] Matlab first-order optimality. [online]. [cited 2019-05-05] Available at: https://www.mathworks.com/help/optim/ug/first-order-optimality-measure.html.

[43] Matlab fmincon interior point algorithm. [online]. [cited 2019-05-06] Available at: https://www.mathworks.com/help/optim/ug/constrained-nonlinear-optimization-algorithms.html#brnpd5f.

[44] Cynthia H O'Callaghan, A Morris, Susan M Kirby, and AH Shingler. Novel method for detection of β-lactamases by using a chromogenic cephalosporin substrate. *Antimicrobial agents and chemotherapy*, 1(4):283–288, 1972.

[45] Zhangming Mao, Feng Guo, Yuliang Xie, Yanhui Zhao, Michael Ian Lapsley, Lin Wang, John D Mai, Francesco Costanzo, and Tony Jun Huang. Label-free measurements of reaction kinetics using a droplet-based optofluidic device. *Journal of laboratory automation*, 20(1):17–24, 2015.

[46] Michael E Lee, William C DeLoache, Bernardo Cervantes, and John E Dueber. A highly characterized yeast toolkit for modular, multipart assembly. *ACS synthetic biology*, 4(9):975–986, 2015.

[47] Austin T Raper, Anthony A Stephenson, and Zucai Suo. Functional insights revealed by the kinetic mechanism of crispr/cas9. *Journal of the American Chemical Society*, 140(8):2971–2984, 2018.

[48] Hanhui Ma, Li-Chun Tu, Ardalan Naseri, Maximiliaan Huisman, Shaojie Zhang, David Grunwald, and Thoru Pederson. Crispr-cas9 nuclear dynamics and target recognition in living cells. *J Cell Biol*, 214(5):529–537, 2016.

[49] Samuel E Clamons and Richard M Murray. Modeling dynamic transcriptional circuits with crispri. *BioRxiv*, page 225318, 2017.

[50] Vlatko Stojanoski, Dar-Chone Chow, Liya Hu, Banumathi Sankaran, Hiram F Gilbert, BV Venkataram Prasad, and Timothy Palzkill. A triple mutant in the ω-loop of tem-1 β-lactamase changes the substrate profile via a large conformational change and an altered general base for catalysis. *Journal of Biological Chemistry*, 290(16):10382–10394, 2015.

[51] DM Mueller and GS Getz. Steady state analysis of mitochondrial rna after growth of yeast saccharomyces cerevisiae under catabolite repression and derepression. *Journal of Biological Chemistry*, 261(25):11816–11822, 1986.

A Materials and methods

A.1 Yeast strains.

Yeast strain used for assays was BY4741 (MATa Δfar1 Δbar1 his3Δ1 leu2Δ0 met15Δ0 ura3Δ0). Firstly, a plasmid carrying BLA on pGRR promoter was integrated into the strain using High efficient yeast transformation. This strain was used for pGRR promoter characterization after pheromone induction. dCas9-Mxi on pFIG1 pheromone-inducible promoter was then integrated into this strain. Finally, different kinds of sgRNA constructs were integrated to create a library of sgRNA mutant strains.

A.2 Plasmid construction.

All plasmids were constructed using Golden Gate technology, specifically MoClo cloning method [46].

- **pFIG1-dCas9-Mxi1-URA3** dCas9 was created from Cas9 by double assembly, using PCR products, that mutated Cas9 sequence (mutations H840A, D10A). dCas9 was than fused to Mxi1 domain [1] (ordered as GBlock) and placed under control of pFIG1 promoter on a backbone carrying uracil marker.
- **pGRR-FLP-BLA-HIS3** pGRR promoter ($pGRR_{5,7}$) was ordered as a GBlock [16]. FLP sequence (allows BLA transport from the cell) was fused to TEM1 β-lactamase sequence, and placed on pGRR promoter on a backbone carrying histidine marker.
- **sgRNA-r5-LEU2** Spacer sequence r5 was taken from [16] and ordered as primers and amplified. Cassette for sgRNA expression from MoClo kit [46] was amplified by PCR and cloned into integration backbone with leucine marker.
- **sgRNA-r5-LEU2 mutants** Mutated sgRNA sequences were taken from [12], ordered as primers and amplified. Fragments were then cloned into previously created sgRNA cassette carrying leucine marker.

B Used parameters

Table B.1: Pulse model parameters.

Name	Value	Description	Source
l_1	$3.7460 \cdot 10^{-4}\, nM^{-1}s^{-1}$	Ste12a and pFIG1 association rate	[2]
l_2	$0.03\, s^{-1}$	Ste12a.pFIG1 dissociation rate	[2]
l_3	$3.7460 \cdot 10^{-4}\, nM^{-1}s^{-1}$	Ste12a and pGRR association rate	[2]
l_4	$1.1\, s^{-1}$	dCas9 production rate from Ste12a.pFIG1	this work
l_5	$0.03\, s^{-1}$	Ste12a.pGRR dissociation rate	[2]
l_6	$1.0433\, s^{-1}$	BLA production rate from Ste12a.pGRR	this work
l_7	$1 \cdot 10^{-3}\, nM^{-1}s^{-1}$	sgRNA.dCas9 and Ste12a.pGRR association rate	[47]
l_8	$2.9 \cdot 10^{-4}\, s^{-1}$	sgRNA.dCas9.Ste12a.pGRR dissociation rate into sgRNA.dCas9 and Ste12a.pGRR	[48]
l_9	$0.9433\, s^{-1}$	BLA production rate from sgRNA.dCas9.Ste12a.pGRR	this work
l_{10}	$3 \cdot 10^{-3}\, nM^{-1}s^{-1}$	sgRNA.dCas9 and pGRR association rate	
l_{11}	$2.9 \cdot 10^{-4}\, s^{-1}$	sgRNA.dCas9.pGRR dissociation rate	[48]
l_{12}	$0.0017\, s^{-1}$	BLA production rate from sgRNA.dCas9.pGRR	this work
l_{13}	$0.0234\, s^{-1}$	BLA production from pGRR	this work
l_{14}	$3.7460 \cdot 10^{-4}\, nM^{-1}s^{-1}$	Ste12a and sgRNA.dCas9.pGRR association rate	[2]
l_{15}	$0.03\, s^{-1}$	Ste12a.sgRNA.dCas9.pGRR dissociation rate into Ste12a and sgRNA.dCas9.pGRR	[2]
l_{16}	$1.8 \cdot 10^{-3}\, nM^{-1}s^{-1}$	sgRNA and dCas9 association rate	[49]
1_{17}	$0\, s^{-1}$	sgRNA.dCas9 dissociation rate	[49]
k_1	$0.1\, nM^{-1}s^{-1}$	Ste12 activation rate	[33]
k_2	$10\, nM$	Ste12 activation rate	this work
k_3	$0.011\, s^{-1}$	Ste12a deactivation rate	this work
m	2	Ste12a cooperativity (pFIG1)	[21]
n	1	Ste12a cooperativity (pGRR)	this work
p	1	sgRNA.dCas9 cooperativity	this work
q	2	Fus3PP cooperativity	this work

Table B.2: Fus3PP approximation parameters.

Name	Value	Description	Source
a_1	5130.6	peakTime Hill function coefficient	this work
a_2	3095.3	peakTime Hill function coefficient	this work
a_3	5.6	peakTime Hill function coefficient	this work
a_4	300	peakTime Hill function coefficient	this work
b_1	26.4	peakValue Hill function coefficient	this work
b_2	4346.7	peakValue Hill function coefficient	this work
b_3	17.3	peakValue Hill function coefficient	this work
b_4	3	peakValue Hill function coefficient	this work
c_1	6.5	parameter k Hill function coefficient	this work
c_2	3000	parameter k Hill function coefficient	this work
c_3	3.5	parameter k Hill function coefficient	this work
c_4	1.25	parameter k Hill function coefficient	this work
t_{shift}	$2000\,s$	peakTime shift lower boundary	this work
T_{shift}	$720\,s$	peakTime shift	this work

Table B.3: Other parameters and used constants.

Name	Value	Description	Source
k_{cat}	$714\,s^{-1}$	enzyme kinetic parameter for hydrolysis of nitrocefin by BLA	[50]
k_M	$30000\,nM$	enzyme kinetic parameter for hydrolysis of nitrocefin by BLA	[50]
V_1	$29\,\mu m^{-3}$	cell volume	[19]
	$3 \cdot 10^7$	number of cells in 1ml (OD600 = 1)	[39]
	0.03	β-lactamase normalization unit	this work
K	7.0747	P^* scaling parameter	this work

Table B.4: Initial concentrations

Name	Value	Source
pGRR	$0.0395\,nM$	this work
pFIG1	$0.0395\,nM$	this work
sgRNA	$39\,nM$	[51]
dCas9	$0\,nM$	this work
Ste12a	$0\,nM$	this work
sgRNA.dCas9	$0\,nM$	this work
Ste12a.pGRR	$0\,nM$	this work
Ste12a.pFIG1	$0\,nM$	this work
sgRNA.dCas9.pGRR	$0\,nM$	this work
sgRNA.dCas9.Ste12a.pGRR	$0\,nM$	this work
BLA	$0\,nM$	this work

C List of abbreviations

CRISPR clustered regularly interspaced short palindromic repeats

DNA deoxyribonucleic acid

RNA ribonucleic acid

PAM proto-spacer adjacent motif

sgRNA single guide RNA

dCas9 dead Cas9

PRE pheromone response element

IFFL incoherent feed-forward loop

pGRR $pGRR_{5,7}$ promoter

Fus3PP phosphorylated Fus3 protein

Ste12a activated Ste12 protein

OD optical density

ODE ordinary differential equations

BLA β-lactamase

MSE mean square error

PCR polymerase chain reaction